The influence of Al:Nb ratio on the microstructure and mechanical response of quaternary Ni–Cr–Al–Nb alloys

P.M. Mignanelli [a], N.G. Jones [a], M.C. Hardy [b], H.J. Stone [a,*]

[a] Department of Materials Science and Metallurgy, University of Cambridge, Cambridge CB3 0FS, UK
[b] Rolls-Royce Plc., PO Box 31, Derby DE24 8BJ, UK

ARTICLE INFO

ABSTRACT

The influence of Al:Nb ratio on the microstructure and properties of Ni–Cr–Al–Nb alloys has been investigated following long-term exposure at elevated temperatures. The γ' volume fraction, size and lattice misfit were seen to increase with a larger Al:Nb ratio, although these changes resulted in reduced hardness. The change in the critical resolved shear stress (CRSS) associated with strong dislocation coupling was determined to be the dominant strengthening mechanism and increased with decreasing Al:Nb ratio. A distribution of tertiary γ' was observed to be necessary in maximising the mechanical properties of these alloys.

1. Introduction

To comply with increasingly stringent aerospace emissions targets [1,2] gas turbine engine manufacturers are seeking to improve engine efficiency. Engine performance can be enhanced through an increase in the temperature at which the engines are operated or, alternatively, through higher rotational speeds. However, current nickel-base superalloys, used in the hottest sections of the engine, are working close to their physical limits and are unable to tolerate any further increase in temperature or stress [3]. The development of new nickel-base superalloys specifically designed to operate under more demanding conditions is therefore critical to the ongoing advancement of gas turbine engines.

Nickel-base superalloys typically consist of an A1 (Strukturbericht notation) matrix (γ) solid solution, reinforced with a distribution of coherent Ni_3Al, $L1_2$ superlattice precipitates (γ'). Within the microstructure there can be up to three distinct distributions of γ', each with a different size range, composition and effect on properties. Relatively coarse ~ 1 μm (in diameter) primary γ' is formed during alloy manufacture and processing, whilst fine secondary and tertiary γ' (~ 100 nm and < 50 nm respectively) form on cooling from solution and through subsequent ageing heat treatments [4].

The plastic deformation of coherent superlattice precipitates, such as γ', demands the passage of paired dislocations, so that the energy associated with the anti-phase boundary (APB) created by the leading dislocation is minimised by the passage of the trailing dislocation [3,5]. The precipitate size has been shown to be critical in determining the coupling of the dislocation pairs [6]. A dispersion of small γ' will result in weak coupling of the paired dislocations, whereby the dislocations are present in only one distinct precipitate at a time. Conversely, large γ' precipitates will result in strong coupling in which both the paired dislocations are located in a single precipitate. The critical resolved shear stress (CRSS) for any given particle size distribution of γ' will therefore be associated with the dislocation coupling mechanism which is the easiest. Both strong and weak dislocation coupling may be seen in alloys with multimodal γ' distributions, and a maximum in the CRSS can be obtained by a γ' distribution through which deformation by neither strong nor weak dislocation coupling is preferred [4]. As a consequence, the yield behaviour of nickel-base superalloys is strongly influenced by the size and volume fraction of the secondary and tertiary γ' precipitates, whilst the role of the primary γ' is limited to grain boundary pinning, minimising γ grain growth during heat treatment.

Investigation of the relative importance of the secondary and tertiary γ' distributions on alloy strengthening has been wide ranging but the results are contradictory, due to the difficulties in isolating the effects of different γ' distributions and γ grain sizes. In the work of Jackson and Reed [4], it was identified that the tertiary γ' precipitates played the most significant role in the strengthening of Udimet 720Li, with an optimum microstructure containing 40 nm tertiary γ'. In contrast, Balikci et al. [7] observed that a refinement of the secondary γ' size was the predominant factor in determining the strength of IN738. Similarly, an improvement in creep properties of IN738 was also reported with a refined distribution of secondary γ' [8]. Therefore, a more appropriate generalisation would be that a refinement of both the secondary and tertiary γ' distributions, to an optimum size, will lead to an

* Corresponding author. Tel.: +44 1223 334320.
E-mail address: hjs1002@cam.ac.uk (H.J. Stone).

improvement of the mechanical properties. However, care should be taken to avoid monomodal distributions of fine γ′, as these have been associated with a significant loss of alloy ductility [9].

The strengthening effect of the different γ′ precipitate formers Al, Ti, Ta and Nb in nickel-base superalloys has been the subject of considerable research [10–13]. It is well established that increasing the Ti:Al ratio will raise the APB energy of the γ′ [14], which in turn reduces the ease with which dislocations may pass through the material. However, the combined effect of Al and Nb without Ti additions is less well known.

Whilst Al is the predominant γ′ former in nickel-base superalloys, Nb is also known to contribute to the formation of γ′ precipitates, but has been reported to have a limited effect on the γ–γ′ lattice misfit [15]. Therefore, Nb additions increase the γ′ volume fraction, without magnifying the driving force for morphological destabilisation. Nb is also a potent solid solution strengthening element of the γ [16], whilst offering the additional benefit of comparatively sluggish diffusion kinetics in nickel [17], thereby limiting precipitate coarsening rates. Indeed, in a study of Ni–Cr–Al–Ti–Nb–C–B alloys by Guo and Ma [15], it was shown that Nb additions improved the strength of the γ matrix through solid solution strengthening, as well as increasing the APB energy of the γ′.

In this paper, a range of model Ni–Cr–Al–Nb quaternary alloys have been studied in order to systematically investigate the effect of Al and Nb on γ′ precipitation. By limiting the number of alloying elements, in comparison to commercial alloys, the factors influencing the precipitation behaviour are reduced and, therefore, the relative effects of Al and Nb can be characterised and compared.

2. Material and experimental procedures

To investigate the relative potency for γ′ formation, the amount of Al and Nb added to each alloy was set at 10 at%. The total of 10 at% precipitate forming elements was then split systematically with ratios of Al:Nb of 7:3, 6:4 and 5:5. To convey environmental resistance to the alloys, 15 at% Cr was added, which reflects a level typical of current polycrystalline nickel-base superalloys. The nominal compositions of the three alloys are shown in Table 1.

Ingots of the alloys, weighing 500 g, were produced by vacuum induction melting (VIM), using Ni of 99.95% purity, Al of 99.9% purity, Cr of 99.99% purity and a Ni–Nb master alloy produced by Goodfellow Cambridge Ltd. Differential scanning calorimetry (DSC) was performed using a Netzsch 404 high temperature calorimeter, with heating and cooling at a rate of 10 °C/min between room temperature and 1400 °C under an argon atmosphere. The DSC data was acquired from samples in the as-cast solution heat-treated and long term exposed conditions to identify critical transformation temperatures. The γ′ solvi were determined from the first derivative of the signal with respect to temperature, and by comparing the signal of the heating and cooling curves [18].

Following casting, the VIM melts were subjected to a super solvus heat treatment of 48 h at 1200 °C. This temperature was chosen with reference to the DSC data to be high enough to ensure the alloy was in the single, γ, phase field and thereby maximise diffusion in the alloy to optimise homogeneity, whilst being sufficiently lower than the measured solidus to avoid the risk of

incipient melting. Following solution heat treatment, each ingot was sectioned and the compositions measured by inductively-coupled plasma-optical emission spectroscopy (ICP-OES) by IncoTest, UK. The three alloys were sectioned into ∼1 cm³ pieces, encapsulated in glass with an argon atmosphere to reduce oxidation, and heat treated for 1000 h at 600, 700 and 800 °C. Metallographic preparation of the samples was completed to a 0.25 μm finish before electrolytic etching with a 10 vol% phosphoric acid solution at 3–5 V. Secondary electron imaging (SEI) of the heat treated microstructures was conducted using a JEOL 6340 FEGSEM. X-ray diffraction spectra from solid metal samples were acquired using a Phillips X'Pert PW3020 diffractometer using monochromated Cu Kα radiation, between 2θ angles of 60° and 150°. These higher angle measurements were deliberately chosen to enable the separation of the γ and γ′ peaks and allow an experimental assessment of lattice misfit. Analysis of the X-ray data was carried out using a multi-peak fitting procedure in WaveMetrics Igor Pro, which consisted of two pseudo-voigt profiles on a 4th degree polynomial background. Phase lattice parameters were subsequently determined from multiple fitted peak positions using a non-linear least squares minimisation.

Quantitative analysis of the secondary and tertiary γ′ precipitate distributions followed a three stage process outlined in Fig. 1, consisting of (1) identification of the precipitates of interest from the secondary electron images, (2) conversion to a binary image by thresholding and (3) quantitative analysis using the ImageJ software package. To ensure the results were statistically robust, a minimum of 300 precipitates were measured in each sample, from which the volume fraction and maximum diameter were determined. The distribution of precipitate size measurements was binned following the method of Scott [19] and the data fitted with a lognormal function using Igor Pro.

To obtain an estimate of the strength, hardness measurements were performed on the aged samples. Ten hardness measurements were made in each sample using a Vickers hardness indenter with a 20 kg mass and 30 s dwell, and averaged to give a mean hardness. Thermodynamic and physical property calculations of the alloys were completed using the Thermo-Calc and JMatPro software packages with the Thermotech TTNi8 database.

3. Results

The experimentally determined alloy compositions are shown in Table 2. The actual compositions of the alloys were in good agreement with the nominal compositions, with all of the additions being within 0.5 at% of the desired level. The only exception is Cr in the Ni–15Cr–6Al–4Nb alloy, which is 0.73 at% lower than the nominal composition.

To determine the solidus and γ′ solvus temperatures, calorimetry measurements were performed on material in the as-cast, solution heat-treated and solution heat-treated and aged conditions. An example of a typical DSC thermogram of alloy Ni–15Cr–6Al–4Nb in the solution heat-treated condition is shown in Fig. 2 and the data for all three alloys are given in Table 3. The liquidus and solidus temperatures reduced with decreasing Al:Nb ratio, varying from 1390 to 1371 °C and 1316 to 1301 °C respectively. The secondary γ′ solvi also follow the same trend, whilst any variation in the tertiary γ′ solvi is considerably smaller.

SEI micrographs of the heat-treated alloys are shown in Fig. 3. It can be seen from Fig. 3a–c that exposure at 600 °C resulted in a conventional γ–γ′ microstructure for all the alloys. As the Al:Nb ratio was reduced, the precipitate size decreased and a change in the precipitate morphology can be observed. With the highest Al: Nb ratio of 7:3, the γ′ had an octodendritic morphology, which became cuboidal at the intermediate Al:Nb ratio of 6:4, and finally

Table 1
Nominal alloy compositions (at%).

Alloy	Ni	Cr	Al	Nb
7Al–3Nb	75	15	7	3
6Al–4Nb	75	15	6	4
5Al–5Nb	75	15	5	5
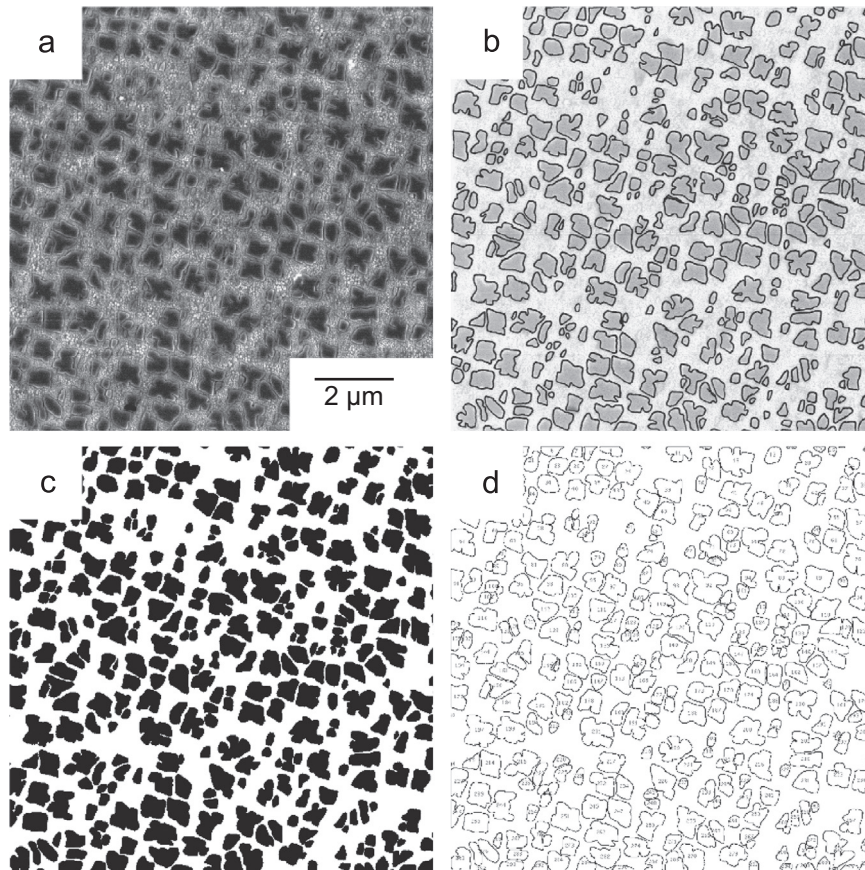
Fig. 1. Example of microstructural characterisation showing (a) the original secondary electron micrograph, (b) the identification of secondary γ′ precipitates, (c) thresholding to a binary image and (d) the analysed precipitate outlines from ImageJ.

Table 2
Actual alloy compositions (at%) determined by ICP-OES at IncoTest, UK.

Alloy	Ni	Cr	Al	Nb
7Al–3Nb	74.92	14.65	7.36	3.07
6Al–4Nb	75.47	14.27	6.34	3.92
5Al–5Nb	75.01	14.67	5.25	5.08

Table 3
The liquidus, solidus, and γ′ solvi temperatures determined by DSC (°C).

Alloy	Liquidus	Solidus	Secondary γ′ solvus	Tertiary γ′ solvus
7Al–3Nb	1390	1316	1088	898
6Al–4Nb	1375	1306	1072	899
5Al–5Nb	1371	1301	1054	895
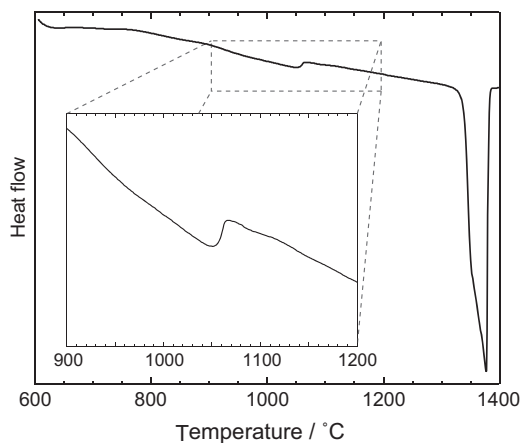
Fig. 2. DSC thermogram of Ni–15Cr–6Al–4Nb following solution heat treatment, with an inset showing a magnified region around the secondary γ′ solvus.

spherical at the Al:Nb ratio of 5:5. These observations suggest that the alloys have different values of lattice misfit between the γ and γ′ phases. In line with the morphologies observed in this study, an increase in lattice misfit has previously been reported to lead to γ′ changing from spherical to cuboidal to octodendritic [20,21]. Also present in the two alloys with the highest Al:Nb ratio are fine tertiary γ′ precipitates, although the apparent absence of tertiary γ′ in Fig. 3c may be the result of a deeper etch than the other samples.

The microstructures following exposure for 1000 h at 700 °C, shown in Fig. 3d–f, resulted in similar trends as those of the samples aged at 600 °C. The finer tertiary γ′, visible after exposure at 600 °C, is prevalent in all three alloys after exposure at 700 °C. This indicates that the tertiary γ′ coarsened considerably with the higher heat treatment temperature and supports the hypothesis that the tertiary γ′ in Fig. 3c may have been etched away.

The microstructures of the alloys following exposure at 800 °C for 1000 h are shown in Fig. 3g-i. The behaviour is markedly different to that of the material exposed at 700 °C. There is a considerable decrease in the secondary γ′ fraction, of between 5% and 10%, from the lower temperature exposures. The secondary γ′ also displays a cuboidal morphology for all three compositions. Furthermore, there is an apparent absence of fine tertiary γ′ precipitates, compared to the microstructures observed at 600 and 700 °C.
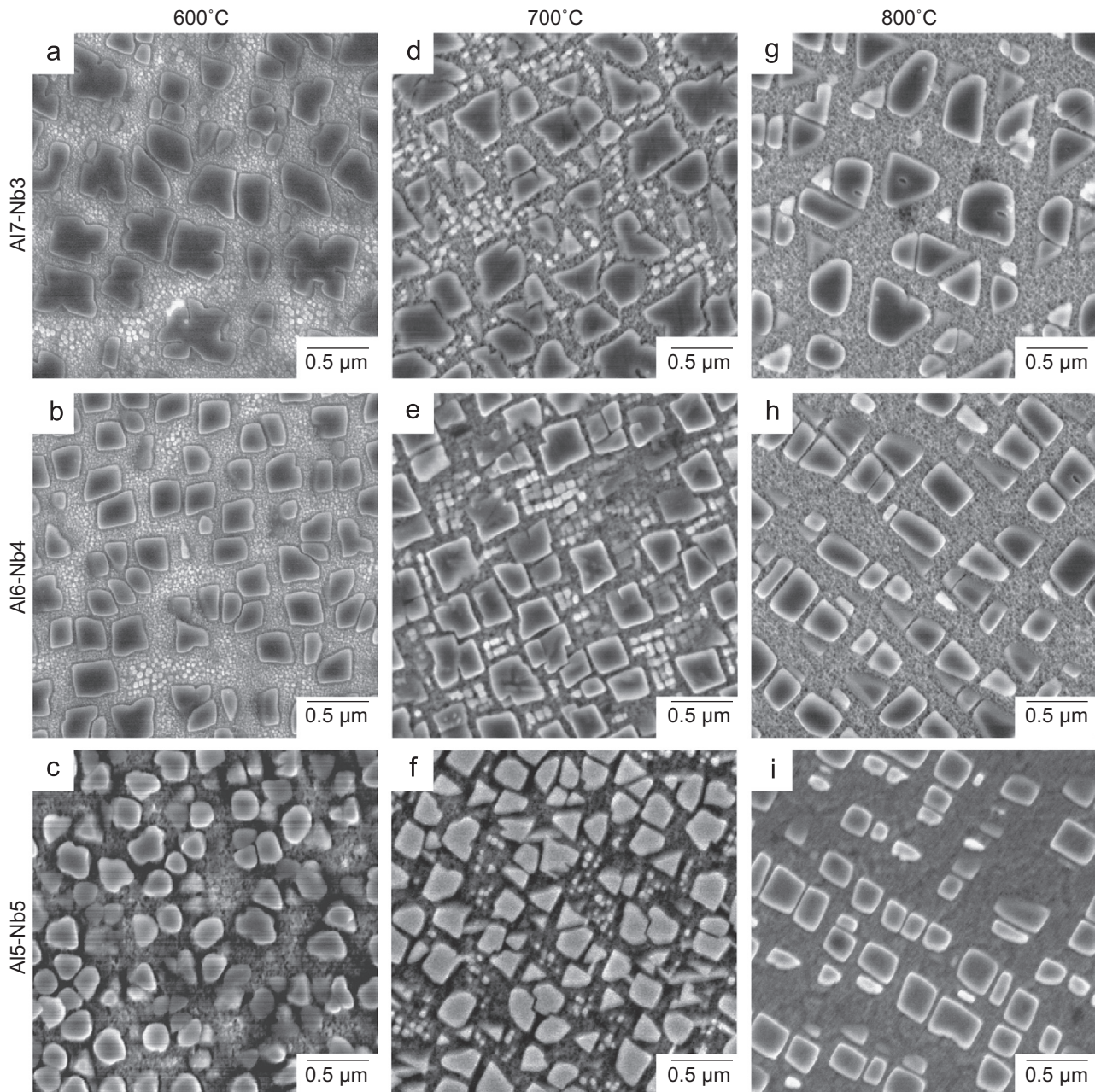
Fig. 3. Secondary electron micrographs of the studied alloys after exposures of 1000 h at 600, 700 and 800 °C.

The lattice misfit of the alloys was assessed via X-ray diffraction and compared with predictions made using the JMatPro software package. The use of higher angle diffraction data enabled sufficient separation of the γ and γ' reflections, such that both contributions could be reliably fitted, as shown in Fig. 4a. Lattice parameters for each phase were determined from multiple fitted peak positions in a non-linear least squares minimisation, and used to calculate the corresponding lattice misfit, presented in Fig. 4b. In general, increasing the Al:Nb ratio of the alloys led to greater lattice misfit between the two phases, although this effect seemed more pronounced at 600 °C than at 700 or 800 °C. A similar effect was also observed with respect to exposure temperature, with the smallest lattice misfit occurring at the lowest temperature. These observations are in good agreement with the γ' precipitate morphologies seen in Fig. 3. In contrast, the lattice misfits obtained using JMatPro, Fig. 4c, predicted that smaller Al:Nb ratios and lower heat treatment temperatures would produce the highest lattice misfit between the two phases.

Thermodynamic calculations of the phase equilibria at each of the three exposure temperatures were completed in Thermo-Calc and the phase fractions obtained are given in Table 4. Comparison of the micrographs and the data presented in Table 4 reveals discrepancies in the predictions across the range of compositions and temperatures studied. The most obvious difference is the absence of δ from any of the experimental microstructures (Fig. 3). This is in direct contradiction to the thermodynamic predictions. To address this issue, further calculations were performed in Thermo-Calc in which only the γ and γ' phases were considered. These results are presented alongside the measured precipitate volume fractions in Fig. 5 as dashed lines.

Fig. 5 shows that the predicted γ' volume fraction obtained using Thermo-Calc increased approximately linearly from 20% to 40% with increasing Al:Nb ratio. The effect of temperature is also
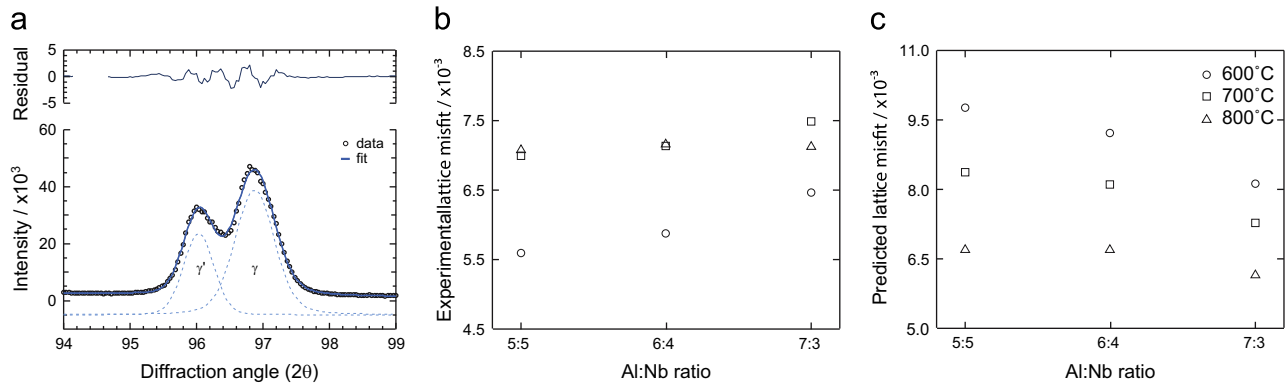
Fig. 4. Measurement of lattice misfit: (a) example of a fitted reflection showing the overall fit, residual curve and the two constituent peak profiles corresponding to the γ and γ′ phases, (b) experimentally determined lattice misfit as a function of alloy composition and heat treatment temperature, and (c) predictions of lattice misfit calculated using the JMatPro software package.

Table 4
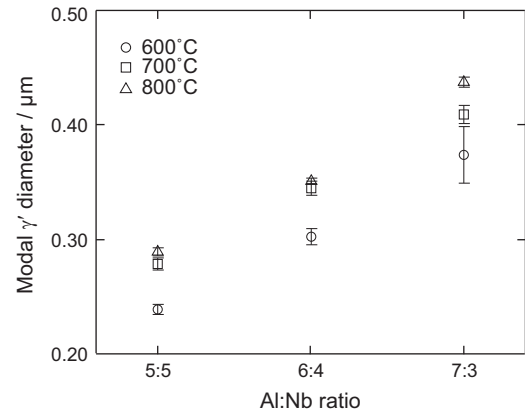Thermo-Calc predicted γ′ and δ phase volume fractions, using the Thermotech TTNi8 database.

	7Al–3Nb		6Al–4Nb		5Al–5Nb	
	γ′ Fraction	δ Fraction	γ′ Fraction	δ Fraction	γ′ Fraction	δ Fraction
600 °C	0.40	–	0.35	0.04	0.27	0.11
700 °C	0.35	–	0.32	0.02	0.24	0.10
800 °C	0.29	–	0.26	–	0.19	0.07
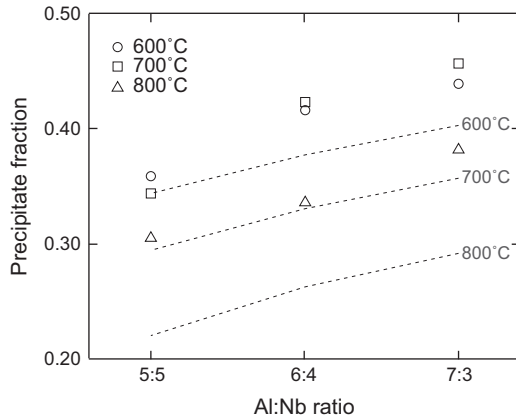
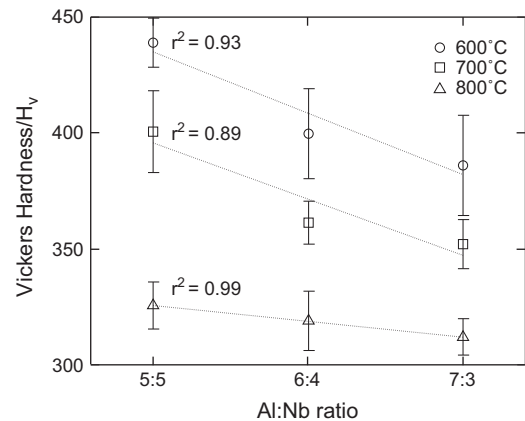
Fig. 5. Comparison of measured (symbols) and Thermo-Calc predicted (dashed lines) γ′ precipitate fractions as a function of Al:Nb ratio following 1000 h heat treatment at 600, 700 and 800 °C.

Fig. 6. Effect of exposure temperature on the secondary γ′ size as a function of Al: Nb ratio.

Fig. 7. Influence of Al:Nb ratio on alloy hardness following 1000 h heat treatment at 600, 700 and 800 °C. The linear fits to the data obtained from each alloy are indicated as dotted lines.

clearly seen, as the precipitate volume fraction decreased with increased temperature. The experimentally determined γ′ volume fraction follows similar trends, with the proportion of γ′ increasing with larger Al:Nb ratios and decreasing with increasing temperature. As the exposure temperature increased, the alloys were closer to their respective γ′ solvus temperatures. This resulted in a concomitant reduction in the γ′ volume fraction, due to increased dissolution of the γ′ phase, as shown in the results in Fig. 5. However, despite the restriction of the Thermo-Calc calculations to a γ–γ′ only microstructure the volume fraction of γ′ phase has been under-predicted across the range of compositions and temperatures considered.

The influence of alloy composition on the secondary γ′ precipitate size is shown in Fig. 6. Higher Al:Nb ratios resulted in an increase in the γ′ size of more than 100 nm at all heat-treatment temperatures. The exposure of the alloys at higher temperatures also produced an increase in the γ′ size for all alloys. However,

Fig. 6 shows that the change in precipitate size is dominated by the variation in Al:Nb ratio, with the exposure temperature having a smaller effect.

Average hardness measurements following heat treatment (symbols) are shown in Fig. 7 alongside a linear fit to the data points (dotted lines). The linear fits resulted in r^2 values of 0.93, 0.89 and 0.99 at 600, 700 and 800 °C respectively. Exposure for 1000 h at 600 °C resulted in an increase in hardness with decreasing Al:Nb ratio of approximately 50 H_v/at% change in Al:Nb. At 700 °C, the change in hardness with Al:Nb ratio mirrors the trends

of the samples exposed at 600 °C, but with a decrease of 45 H_v between the two exposure temperatures. Heat treatment at 800 °C resulted in a similar trend across the composition range, with a smaller change in hardness of only 14 H_v/at%. The effect of increasing exposure temperature from 700 to 800 °C can also be seen to decrease the hardness of these alloys and this change is more pronounced than that observed between 600 and 700 °C, as it decreased by approximately 100 H_v.

4. Discussion

The results of the microstructural characterisation showed that as the Al:Nb ratio was raised, the volume fraction and size of the γ' increased. The higher volume fraction of γ' is a result of the greater potency for γ' formation of Al than Nb. Therefore, although the amount of precipitate formers is constant at around 10 at%, the degree of precipitate formation varies with the Al:Nb ratio. The precipitate size is also strongly related to the Al:Nb ratio, with higher Al:Nb ratios producing larger γ'. The increased kinetics for coarsening and coalescence with higher exposure temperatures also led to an increase in the γ' size, as evident in Fig. 6.

The changes in γ' precipitate morphology observed imply an associated change in the lattice misfit of the alloys [21], which was consistent with the measured values determined by X-ray diffraction (Fig. 4). The predicted values of lattice misfit obtained using JMatPro, suggested that the lattice misfit should increase with smaller Al:Nb ratios at a given temperature. This is in contradiction with the microstructural observations and diffraction measurements, which demonstrate the opposite trend in lattice misfit. However, the experimental results are also in agreement with previous studies that have reported that the Vegard coefficient of Nb in the γ phase is approximately 1.5 times greater than in the γ' phase [22]. Critically, as lattice misfit is known to improve the strength of alloys with coherent precipitates [23], the observation that the hardness is greatest in the alloy with the lowest Al:Nb ratio and spherical precipitates indicates that the lattice misfit is not dominating the strengthening of these alloys.

The under-prediction of the γ' volume fraction of these alloys by Thermo-Calc suggests that the use of thermodynamic software needs to be conducted with some care. Although the system being investigated here includes only four elements, the range of compositions evaluated is quite large and covers an area of composition space that has been the subject of relatively little research. Database development may therefore be required before predictions can be made with appropriate fidelity.

The presence of the tertiary γ', observed in alloy Ni–15Cr–7Al–3Nb after exposure (Fig. 3a, d and g), is a consequence of the proximity of the heat-treatment temperature to the tertiary γ' solvus. In Fig. 3a (600 °C), the tertiary γ' is the smallest, appears to have the largest volume fraction and exhibits a wide range of sizes. In Fig. 3d (700 °C) the size of the tertiary γ' has visibly increased and the volume fraction decreased, whilst Fig. 3g has no resolvable tertiary γ'. The apparent absence of tertiary γ' in Fig. 3g is due to exposure at a temperature close to the tertiary γ' solvus. Any tertiary γ' present in the material exposed for 1000 h at 800 °C has therefore formed during cooling and is consequently of a size below the limit for reliable characterisation using an SEM.

Comparing the results of the hardness tests with the change in γ' size and volume fraction, the evidence suggests that control of the secondary γ' size has the greatest impact upon the strength of each alloy. Conventional wisdom would suggest that an increase in γ' volume fraction would lead to an increase in the hardness of the material. However, in this work the alloys with higher volume fractions of secondary γ' had lower hardness than those with smaller volume fractions of γ'. This indicates that the volume fraction of γ' is not the dominant strengthening mechanism. Critically, the higher hardness material had a smaller γ' size, indicating that a decrease in γ' size may be responsible for the improved hardness. Nevertheless, it should be noted that although the change in precipitate size at 800 °C, Fig. 6, varies in a similar manner to the lower temperature exposures, the change in hardness with composition has a much lower gradient than either of the two lower temperature exposures. This further suggests that the presence of a dispersion of tertiary γ', observed at 600 and 700 °C, is necessary for establishing the strength of nickel-base superalloys, as demonstrated in the work of Locq and Caron [24]. This is also consistent with the work of Jackson and Reed [4] who showed that optimal mechanical properties were achieved at the point where the tertiary γ' was coarse enough to move into the strongly coupled dislocation regime. The presence of a dispersion of tertiary γ' therefore appears important in establishing a high level of strength, whilst the refinement of the secondary γ' size also has a large role in influencing the change in mechanical properties of these materials.

As the strength of superalloys is also known to scale with their APB energy (γ_{APB}) [5], a theoretical assessment of the APB energies was completed. APB energies were determined from the thermodynamic databases using the approach of Miodownik and Saunders [25], which uses the enthalpy of formation obtained from thermodynamic databases and the Bragg–Williams method [26] to correlate the relationship between the calculated enthalpies and the interaction coefficients of the three nearest neighbours. The calculated equilibrium γ' compositions are given in Table 5. The composition of the γ' varies with the change in Al:Nb ratio, with an increase in the Al or Nb content of the alloy being mirrored by the Al or Nb content in the γ'.

The enthalpy of formation was calculated in Thermo-Calc using the TTNi8 database for the ordered γ' and the disordered γ' (γ with the γ' composition) from which the APB energies were calculated (Table 5). It can be seen that a reduction in the Al:Nb ratio is predicted to result in a smaller APB energy. The APB energy was also predicted to decrease with increasing temperature, although the change is very small, varying only in the range 193–199 mJ m^{-2}.

The predicted decrease in APB energy with Al:Nb ratio contradicts the work of Guo and Ma [15] in which the APB energy increased with increasing additions of Nb. However, the alloys in reference [15] had fixed Al and Ti contents and it is therefore thought that the reduction in Al content used to balance the increasing Nb in this work has a larger effect on the rate of change of APB energy than the increasing Nb content [27].

The strengthening afforded by dislocation interaction with precipitates was calculated using the formulae summarised in the work of Kozar et al. [28]. For weakly coupled dislocations the

Table 5
Effect of alloy composition and temperature on the Thermo-Calc predicted γ' compositions (at%), and calculated APB energies.

Alloy	Temperature (°C)	Aluminium	Chromium	Niobium	Nickel	γ_{APB} (mJ m^{-2})
7Al–3Nb	600	15.18	3.42	6.45	74.95	199.3
6Al–4Nb	600	14.12	2.55	8.34	74.99	197.9
5Al–5Nb	600	12.95	2.06	10.00	74.99	193.7
7Al–3Nb	700	15.34	3.31	6.44	74.91	199.2
6Al–4Nb	700	14.34	2.64	8.09	74.93	197.5
5Al–5Nb	700	13.33	2.25	9.52	74.90	193.5
7Al–3Nb	800	15.53	3.24	6.40	74.83	198.6
6Al–4Nb	800	14.62	2.74	7.82	74.82	196.5
5Al–5Nb	800	13.74	2.43	9.05	74.78	192.8
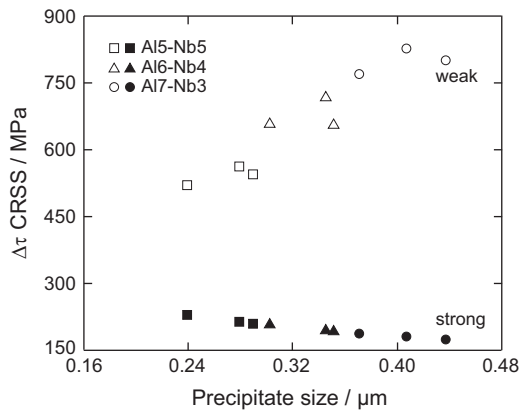
Fig. 8. Variation of predicted change in the CRSS with Al:Nb ratio and temperature. Open symbols indicate weak dislocation coupling and closed symbols indicate strong dislocation coupling.

change in the CRSS, $\Delta\tau$, may be calculated using

$$\Delta\tau = \frac{1}{2}\left(\frac{\gamma_{APB}}{b}\right)^{3/2}\left(\frac{bd_s\varphi}{T}\right)^{1/2}A - \frac{1}{2}\left(\frac{\gamma_{APB}}{b}\right)\varphi \tag{1}$$

where b is the Burgers vector, d_s is the precipitate size, φ is the precipitate fraction, T is the line tension and A is a geometrical factor, which is taken to be 0.72 in the case of spherical precipitates.

Similarly, the change in the CRSS associated with strongly coupled dislocations may be calculated using

$$\Delta\tau = \frac{1}{2}\left(\frac{Gb}{d_s}\right)\varphi^{1/2}0.72w\left(\frac{\pi d_s\gamma_{APB}}{wGb^2} - 1\right)^{1/2} \tag{2}$$

where G is the shear modulus and w describes the repulsion of a pair of dislocations, which can be approximated to a value of 1 [6,29].

To correlate the effect of the changing precipitate distributions and APB energies with the observed hardness results, the changes in CRSS were calculated using Eqs. (1) and (2) for the secondary γ' precipitates. As the shear modulus of the alloys studied here is unknown, the value of a current nickel-base superalloy, RR1000, was used. This reflects the likely properties of these alloys and correlates well with the theoretical values of shear modulus for binary and ternary alloys available in the literature [30–32].

The results of the calculation of the change in the CRSS from the secondary γ' precipitates as a function of alloy composition and temperature are shown in Fig. 8. The calculated effect on the change in the CRSS of weakly coupled dislocations can be seen to decrease from 830 to 540 MPa with a diminishing Al:Nb ratio. In contrast, strongly coupled dislocations are predicted to result in an increase in the change in the CRSS from 170 to 230 MPa with decreasing Al:Nb ratio. The smaller change in the CRSS associated with strong dislocation coupling within the secondary γ' precipitates indicates that this deformation mechanism is preferred over weak dislocation coupling.

Similar calculations of the change in the CRSS from the tertiary γ' precipitates suggest that these precipitates contribute approximately 116 MPa at 600 °C and 89 MPa at 700 °C. However, these predictions must be treated with caution as the polydispersivity of the tertiary γ' distribution is broad, increasing the deviation from the statistical mean particle size used in Eqs. (1) and (2). The broad polydispersivity is most apparent in the microstructures of the alloys heat treated for 1000 h at 700 °C, Fig. 3d–f, which all show both larger, coarsened and finer, re-precipitated tertiary γ'. Effective quantification of the contribution made by the tertiary γ' to the change in the CRSS therefore requires the use of an expression for the strengthening effect that can account for the observed

polydispersivity. Critically, the predicted changes in the CRSS associated with the tertiary γ' precipitates are smaller than those calculated from the secondary γ' precipitates over the range of alloys and temperatures studied.

5. Conclusions

The influence of Al:Nb ratio on the microstructure and properties of Ni–Cr–Al–Nb quaternary alloys has been investigated following long-term exposure at elevated temperatures. Exposure for 1000 h between 600 and 800 °C resulted in a γ–γ' microstructure across the range of compositions examined. The distribution of secondary γ' was observed to increase in size and fraction with increasing Al:Nb ratio. A dispersion of fine tertiary γ' was also observed following heat-treatment at 600 and 700 °C. The lattice misfit was seen to increase both with higher Al:Nb ratios and exposure temperatures. The hardness of the alloys was measured after heat-treatment and it was observed that a decrease in γ' size resulted in stronger material, despite a reduction in volume fraction. A distribution of tertiary γ' was also observed to be necessary in maximising the mechanical properties of these alloys. The APB energies and subsequent change in the CRSS were calculated for each alloy and observed to correlate well with the increase in alloy hardness. The results highlight the relative roles of niobium and aluminium in the control of the γ' size and volume fraction, and the subsequent impact upon mechanical properties.

References

[1] European Aeronautics: A Vision for 2020, European Commission, 2001.
[2] Flightpath 2050 Europe's Vision for Aviation, European Commission, 2011.
[3] R.C. Reed, The Superalloys: Fundamentals and Applications, Cambridge University Press, Cambridge, UK, 2006.
[4] M.P. Jackson, R.C. Reed, Mater. Sci. Eng. A 259 (1999) 85–97.
[5] D. Raynor, J.M. Silcock, Met. Sci. J. 4 (1970) 121–130.
[6] W. Huther, B. Reppich, Z. Metallkunde 69 (1978) 628–634.
[7] E. Balikci, R.A. Mirshams, A. Raman, J. Mater. Eng. Perform. 9 (3) (2000) 324–329.
[8] M. Aghaie-Khafri, M. Hajjavady, Mater. Sci. Eng. A 487 (2008) 388–393.
[9] D.M. Collins, H.J. Stone, Int. J. Plast. 54 (2014) 96–112.
[10] J.K. Tien, J.P. Collier, G. Vignoul, Superalloys 718, 625, 706 and Derivatives, 1989, pp. 553–566.
[11] Z.-Y. Meng, G.-C. Sun, M.-L. Li, X. Xie, Superalloys 1984, AIME, 1984, pp. 563–572.
[12] Y. Xu, L. Zhang, J. Li, X. Xiao, X. Cao, G. Jia, Z. Shen, Mater. Sci. Eng. A 544 (2012) 48–53.
[13] G.N. Maniar, J.E. Bridge Jr., H.M. James, G.B. Heydt, Metall. Trans. 1 (1970) 31–42.
[14] R.F. Miller, G.S. Ansell, Metall. Trans. A 8 (1977) 1979–1991.
[15] E.C. Guo, F.J. Ma, Superalloys 1980, AIME, 1980, pp. 431–438.
[16] Y. Mishima, S. Ochiai, N. Hamao, M. Yodogawa, T. Suzuki, Trans. Jpn. Inst. Met. 27 (9) (1986) 656–664.
[17] M.S.A. Karunaratne, R.C. Reed, Acta Mater. 51 (2003) 2905–2919.
[18] W.J. Boettinger, U.R. Kattner, K.-W. Moon, J.H. Perepezko, DTA and Heat-flux DSC Measurements of Alloy Melting and Freezing, National Institute of Standards and Technology, U.S. Government Printing Office, Washington, 2006.
[19] D.W. Scott, Biometrika 66 (3) (1979) 605–610.
[20] W.T. Loomis, J.W. Freeman, D.L. Sponseller, Metall. Trans. 3 (1972) 989–1000.
[21] R.A. Ricks, A.J. Porter, R.C. Ecob, Acta Metall. 31 (1983) 43–53.
[22] P. Nash, Phase Diagrams of Binary Nickel Alloys, ASM International, Materials Park, Ohio, 1991.
[23] D.A. Grose, G.S. Ansell, Metall. Trans. A 12A (9) (1981) 1631–1645.
[24] D. Locq, M. Marty, P. Caron, Superalloys 2000, TMS, 2000, pp. 395–403.

[25] A.P. Miodownik, N.J. Saunders, Applications of Thermodynamics in the Synthesis and Processing of Materials, TMS 1995, pp. 91–104.
[26] W.L. Bragg, E.J. Williams, Proc. R. Soc. A 145 (1934) 699–730.
[27] R.F. Decker, in: Proceedings of the Steel and Strengthening Mechanisms Symposium, Zurich, 1969.
[28] R.W. Kozar, A. Suzuki, W.W. Milligan, J.J. Schirra, M.F. Savage, T.M. Pollock, Metall. Mater. Trans. A 40 (2009) 1588–1603.
[29] W. Huther, B. Reppich, Mater. Sci. Eng. 39 (2) (1979) 247–259.
[30] K. Chen, L. Zhao, P.C. Patnaik, J.S. Tse, Superalloys 2004, TMS, 2004, pp. 753–758.
[31] D.E. Kim, S.L. Shang, Z.K. Liu, Comput. Mater. Sci. 47 (2009) 254–260.
[32] S.L. Shang, D.E. Kim, C.L. Zacherl, Y. Wang, Y. Du, Z.K. Liu, J. Appl. Phys. 112 (053515) (2012) 1–10.